Assessment of Cooling Capacity by Urban Parks Using a Multi-data Source Approach

Conference Paper · October 2022

3 authors:

Can Trong Nguyen
Charles University in Prague
38 PUBLICATIONS 271 CITATIONS

SEE PROFILE

Amnat Chidthaisong
King Mongkut's University of Technology Thonburi
127 PUBLICATIONS 3,127 CITATIONS

SEE PROFILE

Rungnapa Kaewthongrach
King Mongkut's University of Technology Thonburi
18 PUBLICATIONS 75 CITATIONS

SEE PROFILE

Table of contents

Assessment of Cooling Capacity by Urban Parks Using a Multi-data Source Approach

Can Trong Nguyen[1,2,3], Amnat Chidthaisong[1], Rungnapa Kaewthongrach[3]

[1] The Joint Graduate School of Energy and Environment, King Mongkut's University of Technology Thonburi, Bangkok 10140, Thailand
[2] Faculty of Engineering, Prince of Songkla University (Hatyai campus), Songkhla 90110, Thailand
[3] Space Technology Research Center, Geo-Informatics and Space Technology Development Agency (GISTDA), Chonburi 20230, Thailand
`trongcan.ng@gmail.com`

Abstract. The urban park is a part of urban green infrastructures, essential in urban ecosystems because it delivers various benefits to urban dwellers, from tangible to intangible values. The urban park is widely accepted as a friendly adaptive solution in the context of cities worldwide being warmer due to climate change and urbanization impacts. This research quantified the cooling effect of small and medium-sized parks in Bangkok and identified primary controlling factors. An integrated approach was adopted to achieve the overarching objectives, including image interpretation from various data sources and Trends-Breakpoints Detection Analysis (TBDA). The research findings revealed that summer's most active cooling distance is around 100–200 meters. When the weather is cooler in winter, the cooling distance expands outward to +400 and +1000 meters depending on park structures and neighbouring backgrounds. A park located in a region with denser vegetation is supposed to have a more moderate cooling effect. Increases in tree areas inside a park and their shape complexity can stimulate the cooling effect, especially in the cooler season. In contrast, the cooling effect is only contributed by the park's water surface during the hotter period. The research outcomes are helpful for urban planners in heat mitigation strategies using urban green infrastructures.

Keywords: Urban park, Urban green space, Cooling effect, Cooling distance, Park structure.

1   Introduction

Many studies revealed that Southeast Asia (SEA) cities such as Kuala Lumpur (Malaysia), Bogor (Indonesia), Baguio (Philippines), Yangon (Myanmar), Ho Chi Minh City, and Ha Noi (Vietnam), and Bangkok (Thailand) had overgone the warmer trend in land surface temperature (LST), about 0.03°C to 0.92°C per year (Amanollahi et al., 2016; Estoque & Murayama, 2017; Nurwanda & Honjo, 2019; Son et al., 2017; Srivanit & Hokao, 2012; Tran et al., 2017; Yi et al., 2018). Higher urban temperature is directly responsible for human thermal comfort and heat-related morbidity and mortality in the city (Lowe, 2016; Santamouris, 2020). It also causes pressures on the economy and energy sector for cooling demands, especially during heat waves (Nguyen et al., 2021). Besides, these studies indicated that urban temperature alterations always occur in parallel with urbanization, which induces impervious surface extension and vegetation narrowing. These nexuses imply potential solutions for urban design strategies to reduce the harmful effects of heat exacerbation based on the basic notion of maximizing urban green areas like public parks. In the context of urbanization and escalating climate change, the urban environments are intended to be more severe for their inhabitants. Thus, the role of urban green spaces and public parks in mitigating the urban climate severity is more prominent and apricated by managers and urban dwellers.

On the other hand, large parks frequently attract more attention because they are supposed to have diverse and more significant benefits than small green spaces. In a crowded city, most land budget is prioritized for residential areas and solid urban infrastructures rather than large patches of green spaces (Nguyen & Chidthaisong, 2022). Planning extensive urban forests is challenging. Therefore, we intended to examine the cooling effect of small and medium-sized parks, potentially appropriate for urban greening plans. Additionally, the cooling distance is a principal parameter in the cooling models, e.g., the InVEST-Urban Cooling Model (Hamel et al., 2021). It is diverse and fluctuates from park to park depending on many factors. When the cooling distance is specified, the model performance will significantly improve. The factors controlling the cooling effect will substantially affect a prototype park design to apply to other current and future parks.

This research stands on exploiting diversely free-accessible data to investigate the cooling effect given by the public parks, in which Bangkok is an empirical study. The controlling elements moderating the cooling effect were then analyzed to identify the impacts of the park's structure and the external environment on the cooling effect, which are helpful information for urban planning toward heat mitigation strategies in the city.

2 Study sites and Datasets

2.1 Study sites

Five parks were selected along the urban-periurban gradient of Bangkok (Thailand), considering their popularity and usable area (Fig. 1). The most extensive park is Chatuchak botanical garden which comprises three adjacent parks of Wachira Benchtas, Queen Sirikit, and Chatuchak. Its usable area is 110 ha and has become one of the essential urban green spaces in a compact city like Bangkok. It is followed by Suan Luang Rama IX (shortly Rama 9) with nearly 80 ha. The following two parks are relatively similar in terms of usable area, Lumpini (57.6 hectares) and Serithai (56 ha). However, they own significant disparities in location and park structure. Lumpini is supposed to be a "green asset" in a cramped city, while Serithai has its role in rainwater regulation in the peri-urban of eastern Bangkok. And, Thonburirom (10.058 ha) is located on the city's west side, which plays a crucial role in aesthetics and its surrounding neighbours' environment.
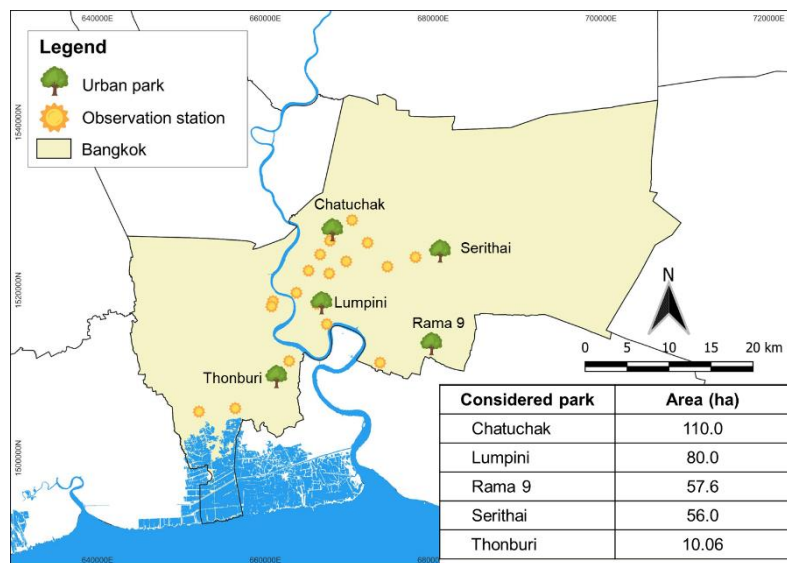
Considered park	Area (ha)
Chatuchak	110.0
Lumpini	80.0
Rama 9	57.6
Serithai	56.0
Thonburi	10.06

Fig. 1. Location of Bangkok, the considered parks, and air quality stations within Bangkok boundary.

2.2   Air temperature data

We obtained air temperature data from the Thailand Pollution Control Department (PCD), which includes 14 stations within the Bangkok metropolitan region. The stations are set up at roadside and ambient locations to hourly measure air temperature. The temperature at each station was selected based on date and time criteria. In particular, we obtained the air temperature at 10:00 am for analysis because the initial test showed that LST and air temperature reached their highest correlation value at 10:00 am.

2.3   Landsat 8 imagery

Landsat 8 (OLI/TIRS) surface reflectance is the primary data source to extract surface characteristics and simulate air temperature from these features. The land surface reflectance (LSR) data is atmospherically corrected using Landsat Surface Reflectance Code. The LSR minimizes atmospheric influences, especially on temperature data, which is relatively susceptible to atmospheric and cloud conditions. We acquired images of clear sky or limited clouds covering the study sites and ambient regions under satisfied weather conditions. Seven scenes were captured at seven milestones from 2014 to 2016 for training and validating the air temperature predictive model. Whereas the clear-sky images acquired on 19/02/2020, 22/03/2020, and 17/11/2020 were adopted to simulate spatial air temperature for further analyses in this study.

2.4   Google Earth-based imagery

The park's landscapes should be classified by very-high-resolution imagery (VHR) since its scale is often small. Yet, we cannot access commercial satellites in this study. Fortunately, Google Earth provides free accessibility to its VHR at different times. Although Google Earth imagery (GEI) cannot offer diverse spectral information as a standard multispectral image, it can adjust the details to be observed. Thus, the GEI becomes a cheaper VHR data source widely

applied in urban studies (Malarvizhi et al., 2016; Mering et al., 2010). We collected GEI at each park using the SASPlanet (v200606) tool. The pixel size of the collected GEI is approximately 0.3 meters per pixel edge.

2.5 Sentinel-2 imagery

GEI is proper for mapping in detail land cover for a small-scale area, it, however, shows limitations in a vast region when the detail of GEI becomes its drawbacks in terms of processing performance. More explicitly, there are potential noises from building shadows, colors of different roof materials, tree canopy structures, and even water surface waves. Therefore, we adopted moderate-high spatial resolution satellite imagery of Sentinel-2 (10 meters) to classify landscape information around the park from its border to 2 km. Sentinel-2 L2A images were collected with an acquisition strategy of the smallest difference in capture date Landsat-8 images above. Two scenes were downloaded directly from the Sentinel Hub on 21/02/2020 (10:37) and 29/08/2020 (10:35). These images have a low cloud coverage rate of 0.47% and 5.81% for the image in February and August.

3 Methodology

3.1 Land cover of the park and surrounding areas

Landscapes of the parks were classified by Google Earth imagery. It comprises five land cover categories: wood tree, grassland, soil/pavement, buildings, and lake/pond. Firstly, the acquired images were reprojected before they were analyzed by object-oriented classification. The images were then overcome through a segmentation procedure, which groups nearby similar pixels together. Segment Mean Shift (SMS) technique was adopted to analyze the GEI. Subsequently, the segmented images were classified by the ISODATA (Iterative Self-Organizing Data Analysis) unsupervised classifier. To cluster pixels into N user-defined groups, the algorithm randomly sets cluster centres and assigns pixels to clusters using minimum distance. The clusters will be merged or split based on the minimum distance among the cluster's centres. The progress is repeated until all pixels are precisely separated, and the number of clusters reaches the user-defined number. In this study, the initial clusters of *N=30* were set for classification. The subclusters were subsequently combined altogether if they presented an identical land cover type when collated with image visualization.

The neighbouring regions of each park were extracted by multispectral imagery of Sentinel-2, which grouped into major land cover categories such as impervious surfaces, vegetation, water bodies, and bare land. The multispectral bands (i.e., visible wavelength, Red-Edge, NIR, and SWIR) were consistently resampled pixel size of 10 meters. Thereafter, we applied integration of principal component analysis (PCA) and ISODATA unsupervised classifier to retrieve park neighbouring land cover. The initial cluster number was defined as *N=15* because Sentinel-2 imagery is less detailed compared to GEI. Finally, the classified images were combined to generate a land cover map based on general land cover types.

3.2 Air temperature estimation using a Machine learning algorithm

Extracting surface characteristics: The surface characteristics were described by spectral indices, which represent three primary land cover patterns, including vegetation, impervious surfaces, and water bodies. Particularly, vegetation was depicted by Normalized Difference Vegetation Index (NDVI) and Enhanced Vegetation Index (EVI). NDVI is a well-known index to identify live green vegetation relating to photosynthetically active radiation (PAR) and Near Infrared (NIR) light (Karnieli et al., 2006; Tucker, 1979). However, it shows limitations when vegetation becomes denser. EVI was proposed to overcome the NDVI limitations by adjusting the NDVI formula by blue light and constants (Liu & Huete, 1995). Hence, we additionally obtained EVI with a desire to separate different vegetation canopies, which are expected to influence the air temperature. The next crucial land cover type is urban features, which mostly contribute to urban warming due to the thermal characteristics of urban materials. We calculated two urban indices (i.e., Urban Index (UI) and Normalized Difference Built-up Index (NDBI)) to test which index better performs for air temperature estimation. The water surfaces were defined by Modified Normalized Difference Water Index (MNDWI) – an optimal water index to locate water features in urban areas (Xu, 2006).

Land surface temperature retrieval. Land surface temperature (LST) was retrieved using a widely applied algorithm, which converts DNs values to LST by calibrating brightness temperature (T_B) using NVDI-based land surface emissivity (LSE) (Eq. 3) (Estoque & Murayama, 2016; USGS, 2016; Weng et al., 2004). Firstly, vegetation fraction (FVC) was calculated by calibrating specific NDVI pixels by NDVI values of fully dense vegetation ($NDVI_V$) and completely bare soil surface ($NDVI_S$) (Eq. 1) (Carlson & Ripley, 1997). Then, LSE was estimated by empirical equations using FVC for Landsat OLI/TIRs (Eq. 2) (Son & Thanh, 2018; Van De Griend & Owe, 1993).

$$FVC = ((NDVI - NDVI_S) / (NDVI_V - NDVI_S))^2 \qquad (1)$$

$$\varepsilon = 0.00149 \times FVC + 0.985481 \qquad (2)$$

$$T_S = (T_B / (1 + (\lambda T_B/\rho)\ln\varepsilon)) - 273.15 \qquad (3)$$

where FVC is vegetation fraction; $NDVI_S$ and $NDVI_V$ are vegetation index of fully dense vegetation and bare soil, respectively; εOLI are land surface emissivity for Landsat OLI; TS is the land surface temperature (^{o}C); TB is brightness temperature in Kelvin; λ is the wavelength of emitted radiance (i.e., Landsat OLI is band 10, $\lambda_{B10} = 10.89 \mu m$); $\rho = hc/\sigma$, with $\rho = 1.438 \times 10^{-2}$ Mk; ε is the land surface emissivity.

Optimal distance determination. Air temperature at a particular location is regulated by its surrounding landscape rather than its land cover. Therefore, we should determine which distance that land cover mostly drives air temperature variation. Firstly, aggregated images of surface indices were generated with the number of pixels on each edge that belongs to an odd number subset $F = \{3,5,6,\ldots, 65,67\}$. These pixels correspond to distances from 90 to 2,100 meters from the stations. The index values were extracted and compared to air temperature at 10:00 a.m. using the Pearson correlation coefficient. The distance of each index was noted when the correlation coefficient achieved the first highest value. The influential distance was subsequently determined as a general distance throughout all indicators. The influential distance is 750 meters.

Air temperature predictive model. LST is a critical variable in air temperature prediction models because it has the most significant relationship with other surface indicators (Hereher & El Kenawy, 2020; Sohrabinia et al., 2015). The best model was detected through a model performance test using cross-validation. Specifically, the simple model of only LST, its combination with each surface indicator, and two other synthetic models of the Random Forest algorithm (RF) were evaluated with iteration N=1000. The most optimal model is determined when a model achieves a higher accuracy with fewer predictors. Finally, the optimally predictive model was applied to its contributors of spatial surface elements to simulate air temperature entirely in study areas.

3.3 Analyzing climate regulation effect

The influential distance of the park was analyzed by trend and breakpoint detection analysis using the green-brown R package (Forkel et al., 2013). Theoretically, the green growth is performed on time series data to explore how the land phenology changes. This study assumed that air temperature variation every 100 meters until 2,100 meters is a node in time series data. The influential distance was detected at a breakpoint where air temperature significantly drops from the park site.

In addition to the LULC area, the landscape metrics, including Percentage of Landscape (PLAND), Aggregation Index (AI), and Landscape shape index (LSI) were computed for park structures and surrounding areas for each 100-meter buffer zone (McGarigal et al., 2012). Subsequently, we analyzed the correlation between air temperature difference (i.e., the gaps between near-park and highly-dense urban areas) and each landscape metric using the Pearson correlation coefficient.

4 Results and Discussions

4.1 Park's land cover structure

Landscapes of the considered parks interpreted from GEI are shown in Fig. 2. Unlike the classic parks only occupied by plants, these parks incorporate diverse landscapes of wood trees, lawns, and water surfaces (Fig.2-A). These designs are based on modern design perspectives to provide rich sceneries and take environmental advantage. In addition to the difference in the usable area, their structures are relatively diverse. The pivotal object throughout the park is vegetation, i.e., it is contributed by any green patch. The tree proportion always maintains from 38.8% (Serithai) to 60.7% (Thonburi) (Fig. 2-B). Lumpini and Chatuchak also hold a rather considerable area of the tree, about 51.9% and 49.2%, respectively. Plus, Chatuchak park is used 30.3% of the usable area for wide lawns, the most extended lawn area among the parks. Regarding the contribution of water surfaces in the parks, Serithai is highlighted with a central lake, where the surface area rate is up to 34.7%.
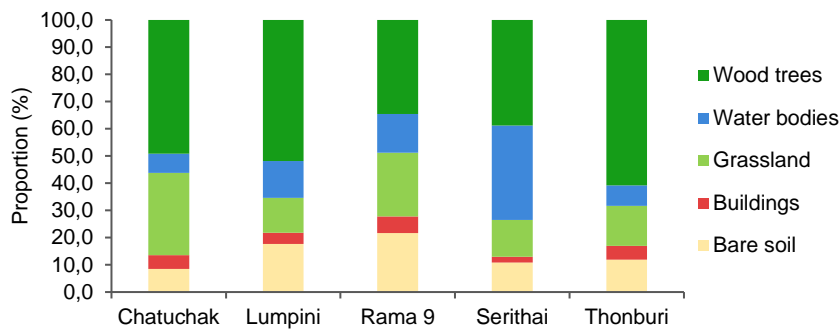
Fig. 2. Landscape proportion in the considered parks delineated from GEI.

4.2 Spatial air temperature

The optimal distance for air temperature simulation was 750 meters. The influential distance was utilized as a buffer distance to extract surface indicators for model testing. Model accuracy for different RF-model combinations is shown in Table 1. Notably, the model with solely LST achieves relatively high accuracy, 0.91 ± 0.028. Adding one or more auxiliary data of surface indicators improves the accuracy of air temperature simulation. Among vegetation indices, the model contributed by EVI is more efficient than the NDVI model, which accuracy is 0.94 versus 0.93 respectively. The models of the urban index are not much different in performance assessed by mean accuracy; nevertheless, the UI model reaches higher maximum accuracy implying potential efficiency compared to NDBI. The model with MNDWI contribution also obtained 0.94 ± 0.02. According to these analyses, we proposed and tested an optimal model (M7), constituted by the favourable elements (i.e., LST, EVI, UI, and MNDWI). Its performance reached a high level of 0.96 ± 0.014 against the above models, with the highest value even achieved at 0.98. The model performance of all elements (M8) is not much distinctive from the M7 model, while the M7 model is able to simulate air temperature with fewer variables. As a result, the M7 model was considered an ideal model for spatial air temperature estimation in Bangkok, $R^2 = 0.91$ and $RMSE = 0.89$. The spatial simulation for air temperature entirely in Bangkok on free cloud dates of 19/02/2020, 22/03/2020, and 17/11/2020 was obtained by applying the ideal M7 model.

Table 2. The accuracy obtained by cross-validation from different models

Model	Predictors	Average Accuracy	Std.
M1	LST	0.906	0.0285
M2	LST, NDBI	0.941	0.0185
M3	LST, EVI	0.932	0.0225
M4	LST, UI	0.942	0.0187
M5	LST, NDVI	0.924	0.0273
M6	LST, MNDWI	0.936	0.0208
M7	LST, EVI, UI, MNDWI	0.954	0.0150
M8	LST, NDBI, UI, NDVI, EVI, MNDWI	0.958	0.0136

4.3 Spatiotemporal distinctness in cooling effect distance

The average Ta within the park boundary extracted from the estimated air temperature is shown in Table 2. Overall, the park air temperature increases from February to March, and in November, it drops to values less than that in February. The highest temperatures throughout the months are at Chatuchak park, while the lowest temperatures are held by Thonburirom park (February and November) and Serithai (November). Regarding temperature variation, for example, here we consider temperature variation between February and March, which shows the most easily variable parks are Lumpini ($\Delta Ta=2.29°C$) and Thonburirom ($\Delta Ta=2.14°C$). On the contrary, Serithai and Rama 9 tend to be more stable in temperature over time, especially Serithai $\Delta Ta=0.55°C$.

Table 3. Average air temperature (°C) at each park in February, March, and November 2020.

Park	February	March	November
Chatuchak	27.678 ± 0.971	29.561 ± 0.879	27.417 ± 1.064
Lumpini	26.893 ± 0.166	29.180 ± 0.367	26.617 ± 0.496
Rama 9	27.087 ± 0.139	28.352 ± 0.522	26.577 ± 0.257
Serithai	27.659 ± 0.252	28.205 ± 0.487	27.989 ± 0.248
Thonburi	26.372 ± 0.035	28.513 ± 0.352	25.283 ± 0.001

We investigated the cooling capacity of each park using breakpoint analysis (Fig. 3). Firstly, the Ta value changes along the horizontal buffer zones from 0 to 2000 meters were assumed and analyzed as annual time series data. Then, the trend and breakpoints were tested to point out the statistically significant trends and breakpoints. The principles accepted for this analysis is the temperature at the park, which is controlled by cooling features such as wood trees, lawns, and water surfaces, being coolest in comparison to surrounding impervious surfaces; plus, the temperature gradually increases under the influences of dense urban areas until the temperature drops again when it reaches rural areas.

Chatuchak is able to control the temperature around the park by about 600±100 meters in November. The influential distance is narrowed from February to March, approximately 200±100 meters (i.e., it can cool up to 400 meters) and 200±100 meters. The Lumpini Park can also cool down its neighbouring areas up to 600±100 meters in winter. Yet, this distance is solely 200 meters in February. In the mid-summer, Lumpini Park does not have a cooling capacity anymore.

Surprisingly, the biggest park of Rama 9 Park has no significant cooling effect through the analysis for both February and March. The cooling effect, however, significantly improves in the winter season. The areas around the park, about 900±100 meters, are mostly affected, and the active distance can expand up to 1200 meters. In Serithai park, only the areas adjacent to the park, about 100 meters, receive the park cooling effect. The affected areas enlarged by 200 meters in November.

In contrast to other parks, i.e., the cooling effect weakens in the mid-summer, the Serithai park shows an outstanding regulative capacity of 500±100 meters. The smallest park of Thonburirom park can reduce the air temperature by around 200 meters and 100 meters in February and March. However, these distances are insignificant. During the winter season, the active cooling distance achieves 1600±100 meters, which is the most extended distance among the considered parks in Bangkok.
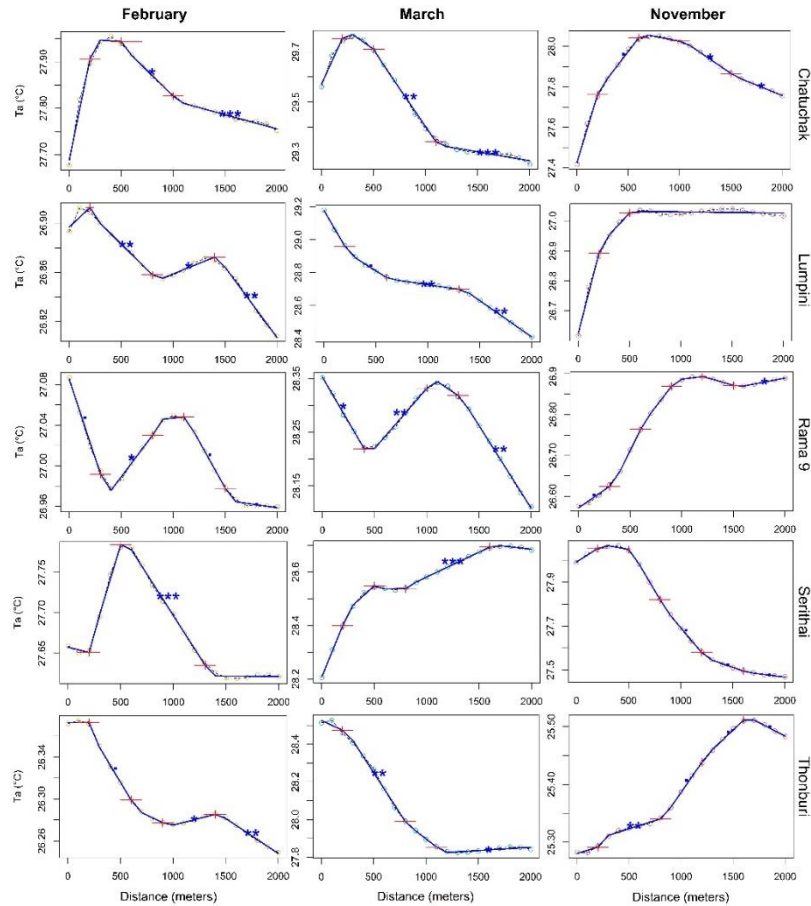

Fig. 3. Temperature changes along horizontal transect and changepoints.

4.4 Pivotal factors regulate park cooling capacity

The park's cooling capacity fluctuates throughout the year depending on seasons, while its inside structures and surrounding environments remain relatively stable simultaneously. Our analyses for temperature variations within 100 meters and 500 meters, 100 meters represent a location cooled down by the park, and 500 meters is a place of denser urban areas (Fig. 4), revealing the parks' temperature and their cooling magnitude are closely associated with location and park structures. For instance, the temperature gap between the two mentioned locations in November (i.e., when all parks' cooling capacities tend to be consistent and clarified) decreases gradually in Chatuchak (0.367°C), Lumpini (0.244°C), Rama 9 (0.13°C), Thonburi (0.042°C), and Serithai (0.016°C). The more significant the temperature gap, the more

41

greatly significantly the park with high cooling capacity is. It means that Chatuchak and Lumpini have higher cooling capacity than other parks.

Fig. 4 shows the background of the parks where they are located. Regarding urban density from 500 meters outwards, Chatuchak and Lumpini stand within the urban areas with the urban density exceeding 50% from 300 meters. Similarly, Serithai and Thonburi are determined to be in peri-urban areas as the urban densities fluctuate around a threshold of 50%. Rama 9 is a suburban park since its surrounding urban density is approximately 35% within the first 1500 meters from the park boundary. The correlation analysis of the park's neighbouring areas influences the park's temperatures and cooling capacity. The results concede that the park cooling capacity is assisted by outside vegetation existence, in which an increase in shape complexity of vegetation patches and green areas is the most meaningful factor. In contrast, the cooling effect is weakened by increasing impervious surfaces.
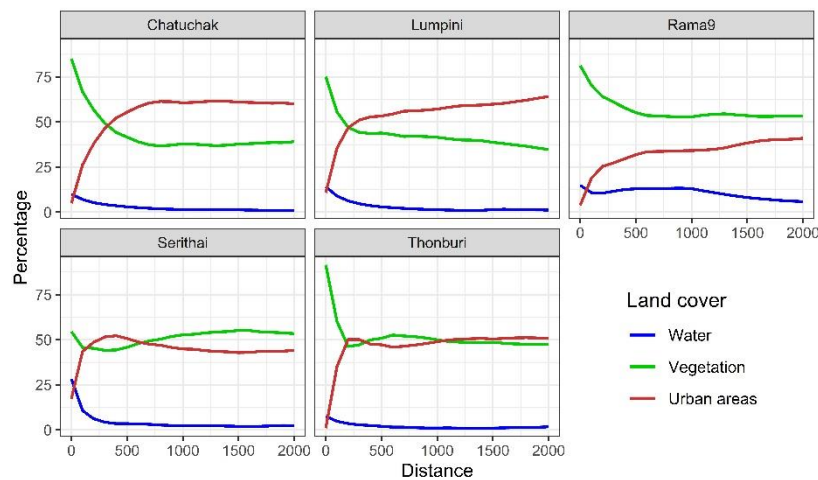

Fig. 4. Proportion of LULC from the park boundary outwards to neighbouring areas.

Regarding the park itself structures, it tends to be more influential in the cooling effect. The tree area is the most statistically significant element controlling cooling intensity (R=0.97, P<0.01). The tree arrangement, i.e., green patches, are planted closely together into plates of complex shapes, which also governs to cool-down park's neighbouring areas. Besides, the water surface area inside the park in the form of a lake and wetland helps to improve the cooling capacity outside the park.

The correlation analysis between the park characteristics, background patterns, and cooling intensity is shown in Fig. 5. The results indicate that both the outside and inside environments drive the cooling effect. In particular, the relationships are more significant in November against February and March. Outside vegetation substantially influences park cooling intensity, with an increase in vegetation proportion (PLAND) and its assembly into big patches (AI, LPI) being the most important determinants. In contrast, the compact impervious surfaces are represented by the spatial metrics of area, proportion, and aggregation, significantly weakening those effects encouraged by green spaces. In terms of the park's structures, the tree area is the most statistically significant factor influencing cooling intensity, notably in November (R=0.97, $P \leq 0.01$). The influence is moderate in February and even non-existent in March. The tree arrangement, i.e., green patches, are planted tightly together to form plates of close and

42

complicated shapes (i.e., AI and LSI), which also cools the park's surrounding regions. Furthermore, the park's water surface area, such as the lake and marsh, aids in improving the cooling capacity outside the park, particularly during the hot season.
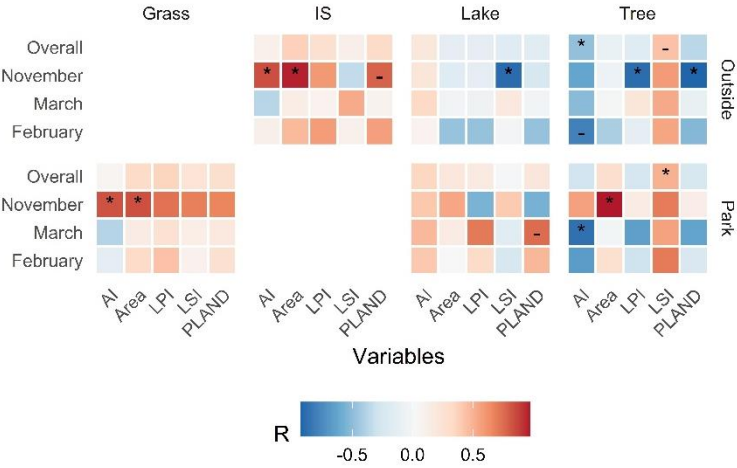

Fig. 5. Heatmap shows correlation coefficients between cooling effect and landscape metrics. Note: Symbols (*) and (-) indicate significance levels at ≤5% and ~10%.

4.5   Implications for urban environment and planning

The considered parks in this study are ranked from small to medium size (10–110 ha). However, the active cooling distance is smaller than about one-third of a 150-ha park (200–300 m) (Hamada & Ohta, 2010) and six times that of a 680-hectare large park (~1400 m) (Yan et al., 2018). Therefore, in urban green space design, small and medium-sized parks placed at the most beneficial distance from each other should be emphasized to maximize the limited urban land budget while ensuring accessibility for all inhabitants. Furthermore, a reasonable distribution of parks with other green infrastructures outside the parks disperses the concentrated pressures, which can improve the cooling effect.

Heat reduction is supported by combining blue and green spaces. Timber trees should be the primary focus. However, water surfaces that play a supportive role, such as a tree-shaded lake and artificial wetland with appropriate aquatic plants, should be applied in urban planning instead of a monotonic and extensive lake. A lawn serves as a venue for outdoor leisure, such as picnics, assemblies, and group activities, and a place to set up the exercise equipment, while a cluster of wood trees decreases air temperature. To minimize monotonic landscapes, the proportions of wood trees, lawns, and lakes within a park should be properly adjusted. The arrangement of trees should be considered, with individual trees being replaced with clusters of trees with intricate forms and edges to increase cooling capacity.

Though landscape integration is important to enrich urban biodiversity and exploit different and beneficial angles, the water surface's cooling effect is prominent in hot weather (Yi et al., 2018). Plus, the effect is reduced at nighttime due to heat release, especially for polluted water in the city. Therefore, in park design, the ratios of vegetated surfaces to water surfaces should be insightfully considered to diversify landscapes and optimize the cooling impact over time.

5   Conclusion

The cooling effect of public parks and the elements that influenced it were investigated. Using multiple data sources, we found integrated landscapes in all parks with a high share of green and blue areas at various combinative ratios. Aside from that, there are differences in cooling distance, which vary according to the season. During the summer, the active cooling distance is usually between 100 and 200 meters. However, the cooling distance extends outward 400 meters and up to 1000 meters, depending on park structures and the surrounding background. The tree area inside the park and the arrangement of green space patches are the most critical factors controlling climate regulation. Although the other neighbouring elements are insignificant in statistics, they are worthily considered in urban planning strategies to mitigate urban heat islands, such as low urban density, high vegetation area, and vegetation shape complexity. Furthermore, the water surface provides an unsteady cooling effect both within and outside the park. As a result, the use of water surfaces as part of a heat mitigation plan should be carefully examined to achieve a more appropriate and sustainable strategy for urban development.

References

[1]   Amanollahi, J., Tzanis, C., Firuz, M., & Makmom, A. (2016). Urban heat evolution in a tropical area utilizing Landsat imagery. Atmospheric Research, 167, 175–182. https://doi.org/10.1016/j.atmosres.2015.07.019

[2]   Carlson, T. C., & Ripley, D. a. (1997). On the relationship between NDVI, fractional vegetation cover, and leaf area index. Remote Sensing of Environment, 62, 241–252. https://doi.org/10.1016/S0034-4257(97)00104-1

[3]   Estoque, R. C., & Murayama, Y. (2016). Quantifying landscape pattern and ecosystem service value changes in four rapidly urbanizing hill stations of Southeast Asia. Landscape Ecology, 31(7), 1481–1507. https://doi.org/10.1007/s10980-016-0341-6

[4]   Estoque, R. C., & Murayama, Y. (2017). Monitoring surface urban heat island formation in a tropical mountain city using Landsat data (1987–2015). ISPRS Journal of Photogrammetry and Remote Sensing, 133, 18–29. https://doi.org/10.1016/j.isprsjprs.2017.09.008

[5]   Forkel, M., Carvalhais, N., Verbesselt, J., Mahecha, M. D., Neigh, C. S. R., & Reichstein, M. (2013). Trend Change detection in NDVI time series: Effects of inter-annual variability and methodology. Remote Sensing, 5(5), 2113–2144. https://doi.org/10.3390/rs5052113

[6]   Hamada, S., & Ohta, T. (2010). Urban Forestry & Urban Greening Seasonal variations in the cooling effect of urban green areas on surrounding urban areas. Urban Forestry & Urban Greening, 9(1), 15–24. https://doi.org/10.1016/j.ufug.2009.10.002

[7]   Hamel, P., Guerry, A. D., Polasky, S., Han, B., Douglass, J. A., Hamann, M., Janke, B., Kuiper, J. J., Levrel, H., Liu, H., Lonsdorf, E., McDonald, R. I., Nootenboom, C., Ouyang, Z., Remme, R. P., Sharp, R. P., Tardieu, L., Viguié, V., Xu, D., … Daily, G. C. (2021). Mapping the benefits of nature in cities with the InVEST software. NPJ Urban Sustainability, 1(1). https://doi.org/10.1038/s42949-021-00027-9

[8]   Hereher, M. E., & El Kenawy, A. (2020). Extrapolation of daily air temperatures of Egypt from MODIS LST data. Geocarto International, 0(0), 1–17. https://doi.org/10.1080/10106049.2020.1713229

[9]   Karnieli, A., Bayasgalan, M., Bayarjargal, Y., Agam, N., Khudulmur, S., & Tucker, C. J. (2006). Comments on the use of the Vegetation Health Index over Mongolia. International Journal of Remote Sensing, 27(10), 2017–2024. https://doi.org/10.1080/01431160500121727

[10]   Liu, H. Q., & Huete, A. (1995). Feedback based modification of the NDVI to minimize canopy background and atmospheric noise. IEEE Transactions on Geoscience and Remote Sensing, 33(2), 457–465. https://doi.org/10.1109/36.377946

[11]   Lowe, S. A. (2016). An energy and mortality impact assessment of the urban heat island in the US. Environmental Impact Assessment Review, 56, 139–144. https://doi.org/10.1016/j.eiar.2015.10.004

[12]   Malarvizhi, K., Kumar, S. V., & Porchelvan, P. (2016). Use of High Resolution Google Earth Satellite Imagery in Landuse Map Preparation for Urban Related Applications. Procedia Technology, 24, 1835–1842. https://doi.org/10.1016/j.protcy.2016.05.231

[13]   McGarigal, K., Cushman, S. A., & Ene, E. (2012). FRAGSTATS v4: spatial pattern analysis program for categorical and continuous maps. Computer software program produced by the authors at the University of Massachusetts.

[14]   Mering, C., Baro, J., & Upegui, E. (2010). Retrieving urban areas on Google earth images: Application to towns of West Africa. International Journal of Remote Sensing, 31(22), 5867–5877. https://doi.org/10.1080/01431161.2010.512311

[15]   Nguyen, C. T., & Chidthaisong, A. (2022). Urban Green Space Inventory using Different Spatial Resolution Satellite Images: Practical notes in Bangkok. The 11th International Conference on Environmental Engineering, Science and Management (pp. 333–340). Environmental Engineering Association of Thailand (EEAT).

[16]   Nguyen, C. T., Diep, N. T. H., & Diem, P. K. (2021). Factors affecting urban electricity consumption: a case study in the Bangkok Metropolitan Area using an integrated approach of earth observation data and data analysis. Environmental Science and Pollution Research, 28, 12056–12066. https://doi.org/10.1007/s11356-020-09157-6

[17]   Nurwanda, A., & Honjo, T. (2019). The Prediction of City Expansion and Land Surface Temperature in Bogor City, Indonesia. Sustainable Cities and Society, 52(2020). https://doi.org/10.1016/j.scs.2019.101772

[18]   Santamouris, M. (2020). Recent progress on urban overheating and heat island research. Integrated assessment of the energy, environmental, vulnerability and health impact. Synergies with the global climate change. Energy and Buildings, 207, 109482. https://doi.org/10.1016/j.enbuild.2019.109482

[19]   Sohrabinia, M., Zawar-Reza, P., & Rack, W. (2015). Spatio-temporal analysis of the relationship between LST from MODIS and air temperature in New Zealand. Theoretical and Applied Climatology, 119(3–4), 567–583. https://doi.org/10.1007/s00704-014-1106-2

[20]   Son, N. T., Chen, C., Chen, C., Thanh, B., & Vuong, T. H. (2017). Assessment of urbanization and urban heat islands in Ho Chi Minh City, Vietnam using Landsat data. Sustainable Cities and Society, 30, 150–161. https://doi.org/10.1016/j.scs.2017.01.009

[21]   Son, N. T., & Thanh, B. X. (2018). Decadal assessment of urban sprawl and its effects on local temperature using Landsat data in Cantho city, Vietnam. Sustainable Cities and Society, 36(2018), 81–91. https://doi.org/10.1016/j.scs.2017.10.010

[22]   Srivanit, M., & Hokao, K. (2012). Thermal Infrared Remote Sensing for Urban Climate and Environmental Studies: An Application for the City of Bangkok, Thailand. Journal of Architectural/Planning Research and Studies, 9(1), 83–100.

[23]   Tran, D. X., Pla, F., Latorre-Carmona, P., Myint, S. W., Caetano, M., & Kieu, H. V. (2017). Characterizing the relationship between land use land cover change and land surface temperature. ISPRS Journal of Photogrammetry and Remote Sensing, 124, 119–132. https://doi.org/10.1016/j.isprsjprs.2017.01.001

[24]   Tucker, C. J. (1979). Red and photographic infrared linear combinations for monitoring vegetation. Remote Sensing of Environment, 8(2), 127–150. https://doi.org/10.1016/0034-4257(79)90013-0

[25]   USGS. (2016). Landsat 8 (L8) Data Users Handbook (LSDS-1574 version 2.0). In USGS Landsat User Services. U.S. Geological Survey.

[26]   Van De Griend, A. A., & Owe, M. (1993). On the relationship between thermal emissivity and the normalized difference vegetation index for natural surfaces. International Journal of Remote Sensing, 14(6), 1119–1131. https://doi.org/10.1080/01431169308904400

[27]   Weng, Q., Lu, D., & Schubring, J. (2004). Estimation of land surface temperature-vegetation abundance relationship for urban heat island studies. Remote Sensing of Environment, 89(4), 467–483. https://doi.org/10.1016/j.rse.2003.11.005

[28]   Xu, H. (2006). Modification of normalised difference water index (NDWI) to enhance open water features in remotely sensed imagery. International Journal of Remote Sensing, 27(14), 3025–3033. https://doi.org/10.1080/01431160600589179

[29]   Yan, H., Wu, F., & Dong, L. (2018). Influence of a large urban park on the local urban thermal environment. Science of the Total Environment, 622–623, 882–891. https://doi.org/10.1016/j.scitotenv.2017.11.327

[30]   Yi, W. C., Hu, B. K. H., Myint, S. W., Feng, C. C., Chow, W. T. L., & Passy, P. F. (2018). Patterns of land change and their potential impacts on land surface temperature change in Yangon , Myanmar. Science of the Total Environment, 643, 738–750. https://doi.org/10.1016/j.scitotenv.2018.06.209